EUROPEAN ORGANIZATION FOR NUCLEAR RESEARCH

CERN/EP 81-25
24 March 1981

# SMALL |t| $\pi^- p$ CHARGE EXCHANGE SCATTERING AT 40 GEV/C

IHEP[1]-IISN[2]-LAPP[3] Collaboration

F. Binon[2], V.A. Davydov[1], S.V. Donskov[1], J. Dufournaud[3], P. Duteil[4], M. Gouanère[3], A.V. Inyakin[1], V.A. Kachanov[1], D.B. Kakauridze[1], G.V. Khaustov[1], Yu. S. Khodirev[1], A.V. Kulik[1], J.P. Lagnaux[2], A.A. Lednev[1], Yu. V. Mikhailov[1], J.P. Peigneux[3], Yu.D. Prokoshkin[1], Yu. V. Rodnov[1], R. Roosen[2], S.A. Sadovsky[1], A.V. Starzev[1], J.P. Stroot[2], V.P. Sugonyaev[1] and A.E. Yakutin[1].

Joint Experiment of IHEP, Serpukhov, USSR

and

CERN, Geneva, Switzerland

Abstract:

$\pi^- p \to \pi^0 n$ differential cross-sections have been measured in the region of small 4-momentum transfer at 40 GeV/c incident momentum. The experiment performed at the IHEP 70 GeV accelerator makes use of a hodoscope $\gamma$-spectrometer. The t-dependence of the cross-section points to a dominance of the spin-flip amplitude.

(Submitted to Zeitschrift für Physik C)

---

1 Institute for High Energy Physics, Serpukhov, USSR.

2 Institut Interuniversitaire des Sciences Nucléaires, Brussels, Belgium.

3 Laboratoire d'Annecy de Physique des Particules, France

4 CERN, Geneva, Switzerland.

JPS/ma

Negative pion charge exchange scattering on protons

$$\pi^- + p \to \pi^0 + n \qquad (1)$$

has been studied at small momentum transfer with 40 GeV/c incident pions in an experiment at high statistical accuracy and low systematic error.

The scattering amplitude of reaction (1) is dominated at high energies by the exchange of the $\rho$ quantum numbers in the t-channel. At small momentum transfer, $|t| < m_\pi^2$, a dip is observed in the differential cross-section with a minimum at $t = 0$, characteristic of spin-flip amplitude dominance [1-5].

Besides high event statistics (more than $10^5 \pi^0$ in the present work) a precise determination of the t-dependence of the differential cross-section at small $|t|$ needs high t-resolution and mininum systematic errors and corrections. The most troublesome of these is due to recoil neutrons from reaction (1) which are detected in the system of counters which is used to reject inelastic events. This correction varies rapidly with t in the region of the dip in the cross-section of reaction (1).

In the first studies of reaction (1) [1-3], statistics were low and the neutron correction anounted to 10-15%, about the same magnitude as the dip in the differential cross-section. The t-resolution at high incident momentum was also not sufficient in the work of Ref. 3. In Ref. 4 the neutron correction is reduced to only a few percent but the statistics are low. Resolution and statistics are achieved in Ref. 5 but the measured neutron correction reached a maximum of 15% [6]. In the present work all three conditions are satisfied together.

The experiment has been performed in the 40 GeV/c negative pion beam of the 70 GeV IHEP accelerator. The lay-out is shown in Fig. 1. The beam is focused on a liquid hydrogen target. Negative pions (and electrons for calibration purposes) are identified with threshold gas Cerenkov counters. The beam particles lateral coordinates are determined to $\pm 0.4$ mm with hodoscopes. Their angle of incidence on the target is measured with a precision of 0.2 mrad. Forward emitted gammas are detected in the hodoscope Cerenkov spectrometer GAMS 200 [7]. A sweeping magnet is installed between GAMS and the target.

GAMS 200 is made of 208 total absorption lead-glass counters (Fig. 2). Its aperture is about a 60 cm diameter circle. The pulses from the counters are measured with a 12-bit ADC system which is linked to a computer through electronics already described [6].

GAMS 200 energy response, which has been studied in electron beams from 1.8 to 40 GeV, is linear to a 1% precision. FWHM resolution is given by the relation $\Delta E/E = 0.027 + 0.125\ E^{-\frac{1}{2}}$ with E in GeV [7].

The algorithms used to determine the coordinates of the gammas (or electrons) in GAMS have been described earlier [7,8]. The precision is

$$\sigma_x = 1.2 \text{ mm}. \tag{2}$$

A detailed description of GAMS 200 is given in Ref. [7].

The thickness of the liquid hydrogen target is 40 cm [9]. The Cerenkov light emitted by the beam particles in the hydrogen is collected on a photomultiplier with a high quantum efficiency cathode, through a bent light funnel. The measurement of the intensity of this light allows for determination of the longitudinal coordinate of the point of a $\pi^- p$ interaction leading to neutral final states

$$\pi^- + p \to M^0 + n \tag{3}$$

with a precision of ±3 cm (Fig. 3) (see Appendix [6,10]).

The hydrogen target is surrounded by a system of guard counters (Fig. 4). This system helps to identify type (3) processes and to reject inelastic ones, like $\pi^- p \to \pi^0 N^{*0}$, $\pi^- p \to \pi^0\pi^0 n$, etc. It includes Cerenkov shower counters which have low efficiency for neutrons emitted in processes like (1) and (3), but which have high $\gamma$ efficiency. This makes it possible to keep the neutron correction in the percent region so as to avoid possible systematic errors in the small $|t|$ cross-section determination.

Each of the 72 $O_i$ counters is a prism of heavy lead glass $TF_5$ (1.8 cm radiation length) on the base of which a photomultiplier is glued. Counters $D_i$ and $G_i$ are built in a similar way. The signals of these counters are analyzed in an ADC system, together with the signals of GAMS counters. Furthermore, the signals of all guard counters are brought into the electronic logic and into registers which are read in the computer.

The trigger signal for the measurement of reaction (1) cross-sections results from the anticoincidence of counters B, $F_1$, $F_2$, A, O, D and G with beam counters $S_{1-5}$. Counters A, O, D and G are removed from the trigger when neutron and other corrections are measured. For each trigger, the amplitudes of the signals of all 208 GAMS counters and all 96 guard counters (O, D and G) are measured.

The gain stability of all counters is continuously monitored to one percent accuracy during the runs with light pulses from photodiodes [7]. Pulsing occurs at each accelerator cycle. The light is fed through flexible fiberglass light guides (Figs. 2 and 4). The stability of the light diodes is checked by comparison with light pulses from an Americium-24 $\alpha$-source deposited on a plastic scintillator.

The equalization of GAMS and guard system counter signals is performed in a wide muon beam [6,7]. The threshold of the guard system counter shapers is set at $\sim$ 1/3 of the signal from a traversing muon; this corresponds to the energy released by a 60 MeV gamma.

The calibration of GAMS 200 is performed with 25 GeV electrons in a defocused beam which irradiates 12 counters simultaneously. Calibration coefficients $\alpha_j$ are obtained on-line by solving a system of linear equations resulting from the condition of minimal energy resolution:

$$\sum_k \left( \sum_j \alpha_j A_j^{(k)} - E \right)^2 = \text{minimum.} \qquad (4)$$

$A_j$ is the signal amplitude in counter j, E = 25 GeV is the electron energy, k is the number of calibration events. Each counter is also calibrated with a narrow (3 × 3 mm$^2$) beam. Both methods give calibration coefficients which agree up to 1% accuracy.

The liquid hydrogen Cerenkov counter is calibrated and monitored with pions which are not interacting in the target and which are also registered in counter $S_7$, positioned after the sweeping magnet (Fig. 1). $\delta$-rays produced in liquid hydrogen by about 5% of these pions are used to check counters $A_i$.

Software controls are used during the runs to check proper hardware functioning: ADC pedestals, stability and linearity of GAMS and guard counters, data acquisition chain, hodoscope efficiency, beam position and profile, stability of the Cerenkov target counter, etc.

On-line analysis software determines the $\gamma$-multiplicity $m_\gamma$, normalizes counter signal amplitudes $A_j$ with the corresponding calibration coefficients $\alpha_j$ and evaluates the energy of each gamma. Momentum and effective mass of particles decaying into gammas are determined through the method of moments. The width of the $\pi^0$ peak in the two gammas invariant mass spectrum is about 8%. There is practically no background around this peak. The shape of the $\pi^0$ energy spectrum (Fig. 5) is identical with that obtained during electron calibration. This shows that collected events of reaction (1) are free of contributions from inelastic processes.

The last step of on-line analysis is the evaluation of the differential cross-section for different kinematical cuts. Real-time treatment of all events with a mini-computer is possible because GAMS readily gives the momentum-vector of each gamma.

Off-line treatment of events with a $\gamma$-multiplicity of two evaluates the coordinates and the energy of the gammas and makes a kinematical analysis of final states. Only events with a total energy in GAMS larger than 20 GeV which are not accompanied by signals in the guard system (thresholds are 35 MeV for $O_i$ counters and 45 MeV for $D_i$ and $G_i$ counters) are considered. As a consequence, practically all inelastic processes with the emission of two and more $\pi^0$ are discarded. Measurements with different $D_i$ and $G_i$ threshold settings show that their contribution is not more than 2%.

The minimum distance between the two gammas from $\pi^0$ emitted in reaction (1) is 10 cm. They are well separated. Few events with larger multiplicities fall into the acceptance of the spectrometer. This makes it possible to use a fast running algorithm for the search for $2\gamma$ events. The search for showers is first performed with an energy threshold $E_{\gamma min}$ of 1 GeV. About 5% of the $\pi^0$ then appear as single gamma events.

These do not survive further analysis which keeps two-gamma events with $\cos\theta^* < 0.7$ only, i.e. $E_\gamma > 6$ GeV ($\theta^*$ is the polar angle in the c.m.s. of the gamma pair). Other two-gamma events are very asymmetrical $\pi^0 \to 2\gamma$ decays. This fact is verified by looking at single gamma events, at a twice lower threshold.

A group of 4 × 4 counter cells around each shower is then analyzed with a lower threshold $E_{\gamma min} = 0.45$ GeV in order to look for small extra peaks. In most cases no such peak has been found. Events are true $m_\gamma = 2$.

Higher multiplicity ($m_\gamma \geqslant 3$) events are checked for peaks originating from noise and from electronic instabilities, as well as from shower fluctuations. The number of events which are transferred from class $m_\gamma = 3$ to class $m_\gamma = 2$ after this procedure is less than 1%. No $\pi^0$ peak is found in the mass spectrum of three-gamma events evaluated with the method of moments [7]. The fraction of events from reaction (1) unidentified as three-gamma ones is less than 0.2%.

The flat distribution in $\cos\theta^* = |(E_{\gamma 1} - E_{\gamma 2})/(E_{\gamma 1} + E_{\gamma 2})|$ of the two-gamma events which satisfy all tests (Fig. 6) demonstrates the linearity of the energy scale of GAMS for gammas (at small $\theta^*$ the distribution is cut by the aperture of the spectrometer).

The determination of gamma coordinates in GAMS 200 is made according to a method which has been described earlier [7]. In the case of separated showers the amplitudes of four counters around the shower are used. An iteration method is used to separate partially overlapping showers. The coordinates of the highest energy shower is first evaluated approximately. A standard amplitude distribution corresponding to this shower, evaluated from calibration runs, is subtracted from the aggregate, thus leaving the second shower profile and coordinates. After a few iterations the result is stable. Monte Carlo evaluations show that this procedure gives unbiased estimates of both gamma coordinates.

Fitting the distribution of the opening angle $\theta_{\gamma\gamma}$ between $\pi^0$ decay gammas with the precision of coordinate measurement as a free parameter gives a value for this quantity $\sigma_x = (1.4 \pm 0.2)$ mm in agreement with expression (2) (Fig. 7).

The finite size of GAMS cells has no influence on the measurements as it is demonstrated by the isotropy of the distributions of the azimuthal angles, both between the $\pi^0$ and the incident $\pi^-$ and between the $\pi^0$ and its decay gammas (Fig. 8). A Monte Carlo calculation confirms that the procedure for the evaluation of coordinates gives results on differential cross-sections which agree to better than 1% with the input data. The FWHM t-resolution, which essentially depends on the coordinate precision, is given by

$$\delta t = 0.0008 + 0.04 \sqrt{|t|} \ (\mathrm{GeV/c})^2 \qquad (5)$$

$1.5 \times 10^5$ two-gamma events with $\cos \theta^* < 0.7$ (this cut radically reduces the background which mainly occurs at $\theta^* \sim 0$) have finally gone through a 1-c fit procedure (Fig. 9). The $\pi^0$ mass peak has a FWHM of 6.5 %. The background is less than $10^{-3}$. Small corrections have been taken into account for the evaluation of differential cross-sections like particle absorption, accidental anti-coincidences and $\delta$-ray detection in the guard system, contamination of inelastic processes and finite t-resolution. The acceptance of the set-up has been evaluated by Monte Carlo calculations.

The correction for neutrons detected in the guard system has been obtained in ad hoc measurements with counters $A_i$ and $O_i$ not participating in the trigger. The distributions of azimuthal angles between forward emitted $\pi^0$ and one $A_i$ counter with and without a gamma detected in counters $O_i$ are shown in Fig. 10. The lower histogram ("$\gamma$"), representing inelastic events, is described by the sum of a $90^\circ$ FWHM gaussian and of a small uniform background. The upper one ("n") with $A_i$ counters fired only is a narrow peak with a width of $30^\circ$, in agreement with the aperture of $A_i$ counters, superposed on a distribution of type "$\gamma$" (dashed curve). The full curve is evaluated by a Monte Carlo calculation for coplanar events of reaction (1). This process has been repeated for different t intervals. The resulting neutron correction (Fig. 11) does not exceed 1.5% in the interval $0 < |t| \leq 0.3 \ (\mathrm{GeV/c})^2$.

The values of the differential cross-section of reaction (1) are given in the table and are represented in Fig. 12. The total cross-section

has been normalized to $\sigma = (10.4 \pm 0.5)\ 10^{-30}$ cm$^2$ [4,5] (3.6% of events fall in the region $|t| > 0.3$ (GeV/c)$^2$). The t-dependence of the cross-section has also been evaluated with two-gamma events choosen on the basis of a 2-c fit (both the neutron and the $\pi^0$ masses were fixed in the final state, $\chi^2 < 6$). The resulting $d\sigma/dt$ values are in agreement with those obtained on the basis of a 1-c fit.

The differential cross-section of reaction (1) may be parametrized at high energies and small $|t|$ by the relation [3,5].

$$\frac{d\sigma}{dt} = \left(\frac{d\sigma}{dt}\right)_{t=0} (1 - gct)e^{ct}, \tag{6}$$

where g is the ratio between spin-flip and non-spin-flip cross-sections. The depth of the t = 0 dip (expressed as the ratio between the maximum cross-section and its value at t = 0) does not depend on c:

$$R = \left(\frac{d\sigma}{dt}\right)_{tmax} \Big/ \left(\frac{d\sigma}{dt}\right)_{t=0} = g\, e^{\frac{1-g}{g}}. \tag{7}$$

Figure 12 shows that at 40 GeV/c in reaction (1) $R \simeq 1.2$ and $g \simeq 2$ express the spin-flip dominance in agreement with former experiments [5].

The experimental data have been fitted over the whole momentum transfer range $0 < |t| \leq 0.3$ (GeV/c)$^2$. The fitted value of the forward cross-section, normalized to the total cross-section for easy comparison with other experiments

$$\frac{1}{\sigma}\left(\frac{d\sigma}{dt}\right)_{t=0} = (5.26 \pm 0.06)\ (\text{GeV/c})^{-2}, \tag{8}$$

may be compared with $(5.2 \pm 0.5)$ (GeV/c)$^{-2}$ in Ref. [4] and $(5.16 \pm 0.17)$ (GeV/c)$^{-2}$ in Ref. [5].

Other parameter values resulting from the fit with (6) are:

$$\begin{aligned} g &= 2.01 \pm 0.04, \\ c &= (15.8 \pm 0.2)\ (\text{GeV/c})^{-2}. \end{aligned} \tag{9}$$

Error limits in c include geometrical imperfections of the set-up which have been evaluated in an analysis of the azimuthal asymmetry of $\pi^0$ distribution at large $|t|$.

We would like to thank the IHEP and CERN Directorates for their support. We acknowledge C. Bricman and S.S. Gerstein for discussions of the present results.

Table 1

$\pi^- p \to \pi^0 n$ differential cross-sections at 40 GeV/c

| $\|t\|$, $(GeV/c)^2$ | $\Delta t$, $(GeV/c)^2$ | $d\sigma/dt$, $10^{-30}$ $cm^2/(GeV/c)^2$ (*) |
|---|---|---|
| 0.0005 | ± 0.0005 | 54.4 ± 1.7 |
| 0.0015 | | 56.4 ± 1.7 |
| 0.0030 | ± 0.001 | 58.2 ± 1.3 |
| 0.0050 | | 58.8 ± 1.3 |
| 0.0070 | | 59.6 ± 1.3 |
| 0.0095 | ± 0.0015 | 61.3 ± 1.1 |
| 0.0125 | | 63.1 ± 1.1 |
| 0.0155 | | 65.7 ± 1.1 |
| 0.0185 | | 65.7 ± 1.1 |
| 0.0215 | | 64.3 ± 1.1 |
| 0.0245 | | 65.2 ± 1.1 |
| 0.0275 | | 65.4 ± 1.1 |
| 0.0305 | | 67.0 ± 1.1 |
| 0.0340 | ± 0.002 | 66.0 ± 1.0 |
| 0.0380 | | 66.0 ± 1.0 |
| 0.0420 | | 67.1 ± 1.0 |
| 0.0460 | | 65.7 ± 1.0 |
| 0.0500 | | 63.8 ± 1.0 |
| 0.0540 | | 63.0 ± 0.9 |
| 0.0580 | | 62.3 ± 0.9 |
| 0.0625 | ± 0.0025 | 60.7 ± 0.8 |
| 0.0675 | | 58.6 ± 0.8 |
| 0.0725 | | 57.9 ± 0.8 |
| 0.0775 | | 56.9 ± 0.8 |
| 0.0825 | | 53.7 ± 0.8 |
| 0.0875 | | 51.6 ± 0.7 |

(*)

Statistical errors; overall absolute normalisation coefficient: ± 5%.

Table 1 (Cont'd)

| $\|t\|$, $(GeV/c)^2$ | $\Delta t$, $(GeV/c)^2$ | $d\sigma/dt$, $10^{-30}$ $cm^2/(GeV/c)^2$ |
|---|---|---|
| 0.0925 | | 50.4 ± 0.7 |
| 0.0975 | | 47.8 ± 0.7 |
| 0.1025 | | 45.9 ± 0.7 |
| 0.1075 | | 43.6 ± 0.7 |
| 0.1125 | | 41.7 ± 0.7 |
| 0.1175 | | 40.0 ± 0.7 |
| 0.1225 | | 38.7 ± 0.7 |
| 0.1275 | | 37.5 ± 0.7 |
| 0.1325 | | 35.5 ± 0.7 |
| 0.1375 | | 33.9 ± 0.7 |
| 0.1425 | | 32.2 ± 0.7 |
| 0.1475 | | 30.2 ± 0.7 |
| 0.1525 | | 29.0 ± 0.7 |
| 0.1575 | | 28.4 ± 0.7 |
| 0.1625 | | 26.4 ± 0.6 |
| 0.1675 | | 24.7 ± 0.6 |
| 0.1725 | ± 0.0025 | 22.8 ± 0.6 |
| 0.1775 | | 21.2 ± 0.6 |
| 0.1825 | | 20.6 ± 0.6 |
| 0.1875 | | 19.3 ± 0.6 |
| 0.1925 | | 18.8 ± 0.6 |
| 0.1975 | | 18.0 ± 0.6 |
| 0.2025 | | 17.0 ± 0.6 |
| 0.2075 | | 15.6 ± 0.5 |
| 0.2125 | | 14.8 ± 0.5 |
| 0.2175 | | 14.1 ± 0.5 |
| 0.2225 | | 13.2 ± 0.5 |
| 0.2275 | | 11.8 ± 0.5 |
| 0.2325 | | 10.9 ± 0.5 |
| 0.2375 | | 10.6 ± 0.5 |
| 0.2450 | | 10.0 ± 0.3 |
| 0.2550 | | 9.1 ± 0.3 |
| 0.2650 | ± 0.005 | 7.7 ± 0.3 |
| 0.2750 | | 6.7 ± 0.3 |
| 0.2850 | | 5.7 ± 0.3 |
| 0.2950 | | 4.9 ± 0.3 |

APPENDIX

## DETERMINATION OF THE $\pi^-$ POINT OF INTERACTION IN THE TARGET

The emission angle $\theta$ of the Cerenkov light from $\pi^-$ going through the liquid $H_2$ target is 453 mr. It is collected by a cylindrical mirror made of aluminized mylar. The light which is emitted at the entrance of the target is undergoing four to five reflections on the cylinder wall. This number decreases for light emitted further and further along the target. 15% light intensity is lost at each reflection. The quantity of light emitted at a distance z from the target entrance which is finally reaching the photomultiplier may be rather well evaluated through the following absorption-like expression

$$dA \sim e^{b\left(\frac{z}{L}-1\right)} dz , \qquad (A1)$$

where L is the length of the target (40 cm). The coefficient b which takes into account light absorption and reflection losses. It is roughly proportional to $tg\theta.L/d$, the mean number of light reflections for through-going particles, and to the logarithm of the mirror coefficient of reflection. This parameter b is evaluated by fitting experimental data (Fig. 3). Its value is about 1 for the present set-up.

Simple integration gives the value of z for a $\pi^-$ which disappears at point z in a reaction with a neutral final state.

$$z = \frac{L}{b} \ln \left[1 + \frac{A(z)}{A(L)} (e^b - 1)\right] . \qquad (A2)$$

A(z) is the amplitude of the signal of the interacting $\pi^-$ and A(L) is the amplitude of the signal of a non-interacting $\pi^-$ going through the whole target.

Measurement error on z is evaluated through the relation

$$\delta z = \frac{L}{b} e^{-\frac{bz}{L}} \left(e^{\frac{bz}{L}} - 1\right)^{\frac{1}{2}} \left(e^{\frac{bz}{L}} + e^b - 2\right)^{\frac{1}{2}} \frac{\delta A(L)}{A(L)} \qquad (A3)$$

It increases rapidly from $z = 0$ to $z \sim 0.3$ L and it does not depend on z after. With the present set-up, $\delta A(L) / A(L) = 0.12$.

## REFERENCES

[1] I. Mannelli et al., Phys. Rev. Lett. 14, 408 (1965).

[2] A.V. Stirling et al., Phys. Rev. Lett. 14, 763 (1965).

[3] V.N. Bolotov et al., Nucl. Phys. B73, 365 (1974).

[4] A.V. Barnes et al., Phys. Rev. Lett. 37, 76 (1976).

[5] W.D. Apel et al., Nucl. Phys. B154, 189 (1979).

[6] W.D. Apel et al., Nucl. Phys. B152, 1 (1979).

[7] F. Binon et al., IHEP 80-141.

[8] G.A. Akopdjanov et al., Nucl. Instr. and Methods 140, 441 (1977)

[9] N.S. Bezverchnjaja et al., IHEP 77-58.

[10] F. Sergiampietri, International Conference on Instr. in High Energy Physics, 430, Frascati 1973.

FIGURE CAPTIONS

Fig. 1 : Experimental set-up:

$H_2$ : 1 mm step, x-y coordinate hodoscopes,

$S_4$ and $S_5$: last beam defining counters before the liquid hydrogen target $LH_2$,

M : sweeping magnet with screen E,

$F_1$, $F_2$ and A : guard system scintillators,

B : lead-scintillator sandwich,

O : 72 guard system lead-glass shower counters,

D and G : 12 lead glass counters each,

$S_7$ : scintillation counter in the beam swept by magnet M,

GAMS-200 : gamma spectrometer.

Dotted lines show the aperture of the set-up.

Fig. 2 : Schematic view of GAMS-200:

1 : F8 lead glass radiators ($36 \times 36 \times 420$ mm$^3$),

2 : FEU 84-3 photomultipliers,

3 : fiber glass light guides for LED calibration system.

Fig. 3 : Spectrum of the longitudinal coordinate of the $\pi^-$ interaction point in the liquid $H_2$ target measured by the amount of emitted Cerenkov light (reaction (3)). Curve: see Appendix.

Fig. 4 : Guard system:

B : lead-scintillator sandwich

$O_i$, $D_i$ : truncated prism lead-glass counters ($G_i$ counters (fig. 1) are not represented but are identical to $D_i$ ones).

$O_i$ counters: base $9 \times 9$ cm$^2$, height 9 cm,

$D_i$ and $G_i$: base $12 \times 12$ cm$^2$, height 15 cm.

$A_i$ : $0.4 \times 8 \times 60$ cm$^3$ scintillation counters (3 out of 12 are shown). Light collection is uniform to better than 10%.

Figure captions (Cont'd)

1 : FEU-110 photomultipliers,

2 : fiber glass light guides for LED calibration system.

$LH_2$ : external envelope of liquid $H_2$ target,

3 : light guide,

4 : photomultiplier of the liquid $H_2$ Cerenkov counter.

Fig. 5 : $\pi^o$ energy spectrum.

Fig. 6 : Gamma pair distribution as a function of $\cos\theta^*$ for events in the $\pi^o$ peak. $|t| \leq 0.04$ $(GeV/c)^2$. The dotted curve results from a Monte-Carlo calculation. The arrow indicates the $\cos\theta^*$ cut for purpose of analysis.

Fig. 7 : Gamma pair distribution as a function of $\theta_{\gamma\gamma}$ for events in the $\pi^o$ peak. $\theta_{min} \simeq 2\, m_{\pi o}\, c/p$. The curve results from a Monte-Carlo calculation with $\sigma_x = 1.4$ mm. The arrow indicates the $\theta_{\gamma\gamma}$ cut corresponding to $\cos\theta^* = 0.7$.

Fig. 8 : Gamma pair distribution as a function of

a) $\phi_{\pi^o\pi^-}$, the azimuthal angle between the momentum vectors of $\pi^o$ and $\pi^-$;

b) $\phi_{\gamma\pi^o}$, the azimuthal $\pi^o$ decay angle. $|t| < 0.04$ $(GeV/c)^2$.

Fig. 9 : Gamma pair mass spectrum after 1c-fit (neutron mass in reaction (3), $\chi^2 < 2.5$).

Fig. 10 : Azimuthal angle between forward $\pi^0$ and fired $A_i$ counter distribution:
"n": one counter $A_i$ fired only,
"$\gamma$": one $A_i$ and one or two $O_i$ counters fired.
Curves result from fits.

Figure captions (Cont'd)

Fig. 11 : Neutron correction as a function of t. The curve is computed.

Fig. 12 : $\pi^- p \to \pi^0 n$ differential cross-section at $p_{\pi^-} = 40$ GeV/c. t-resolution is shown at the bottom. The curve is a fit of the data with relation (6).

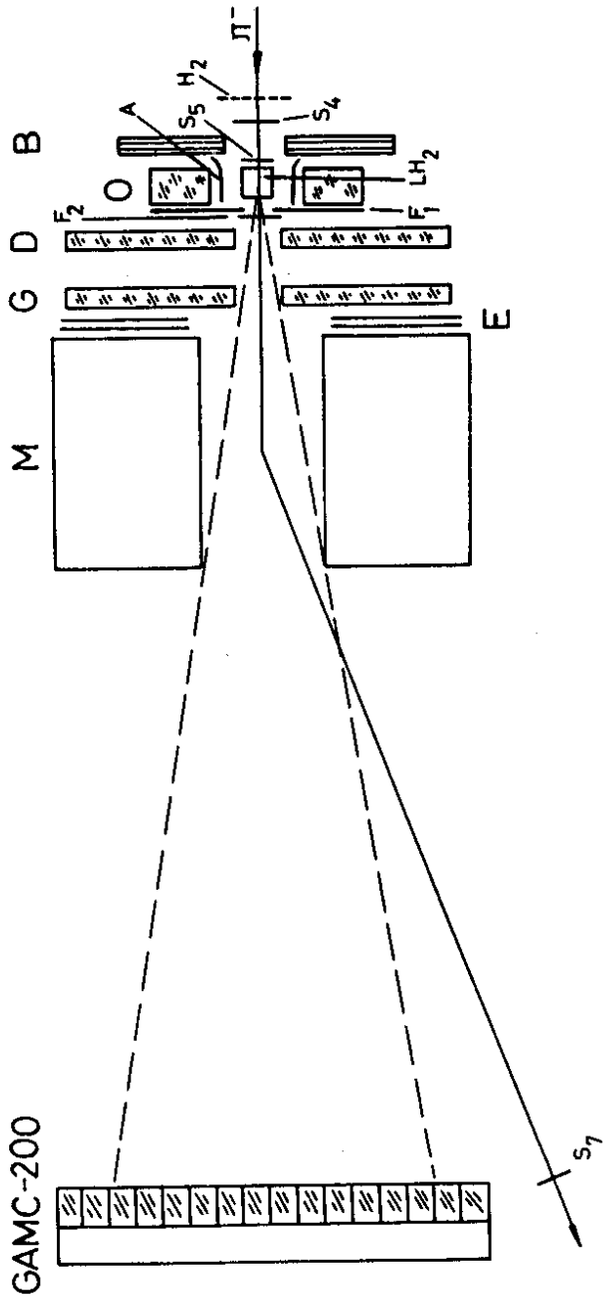


Fig. 1

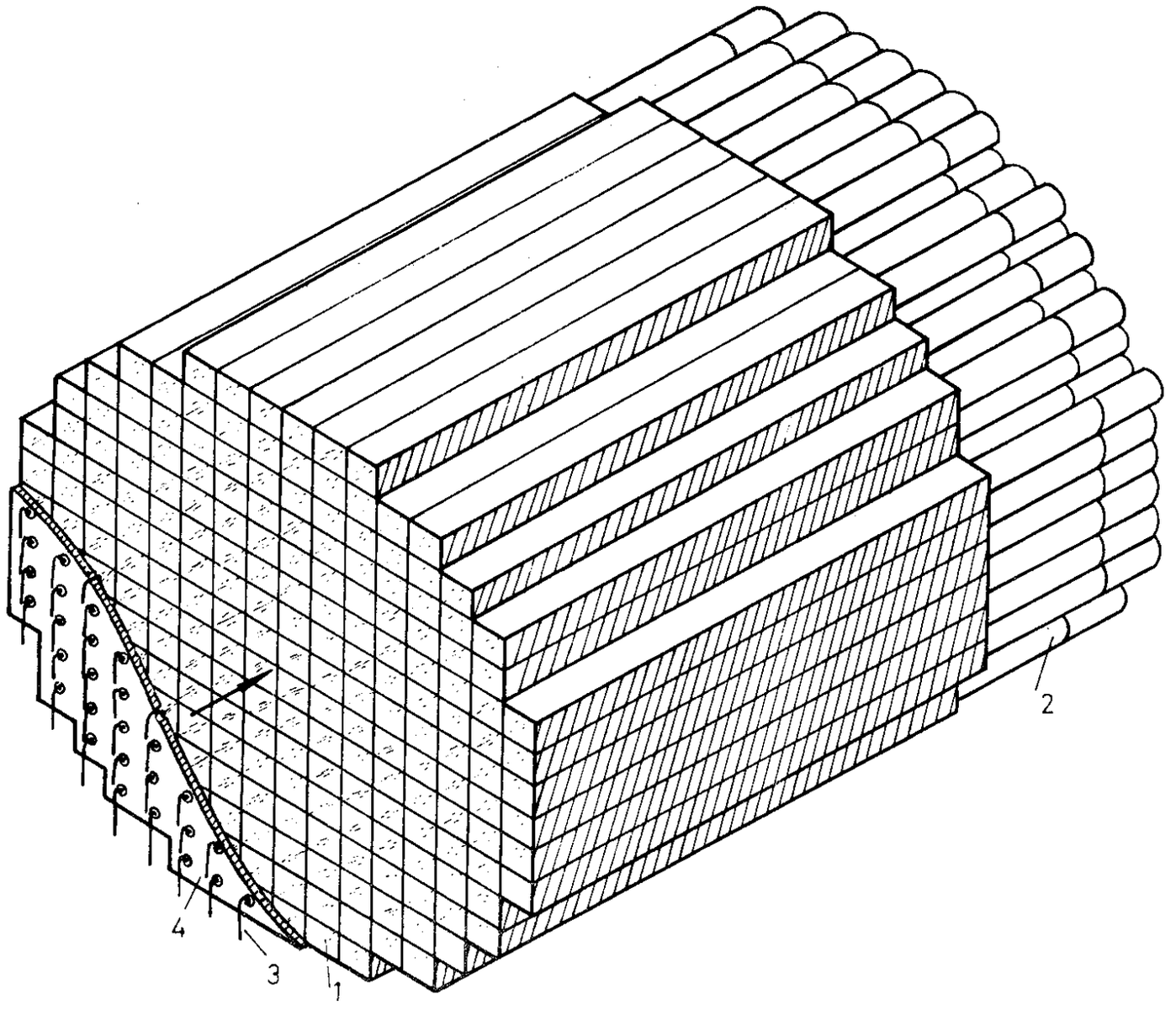


Fig. 2

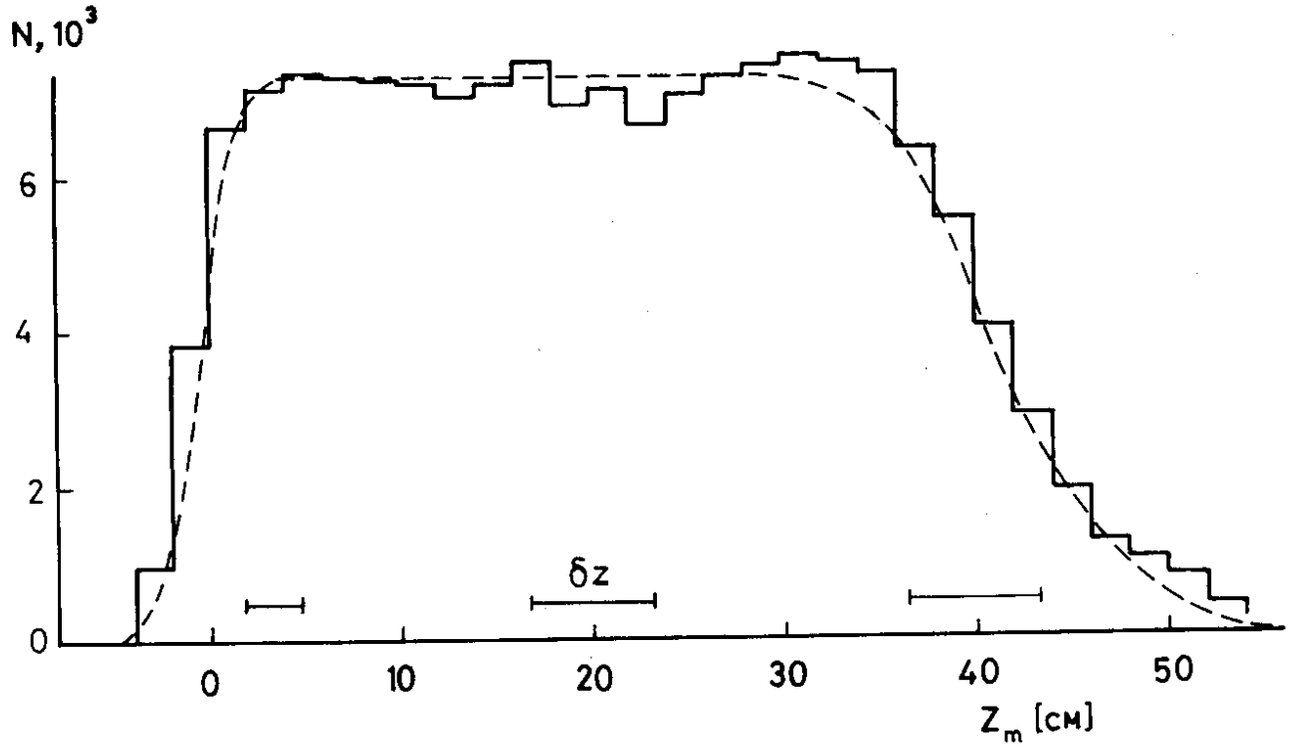


Fig. 3

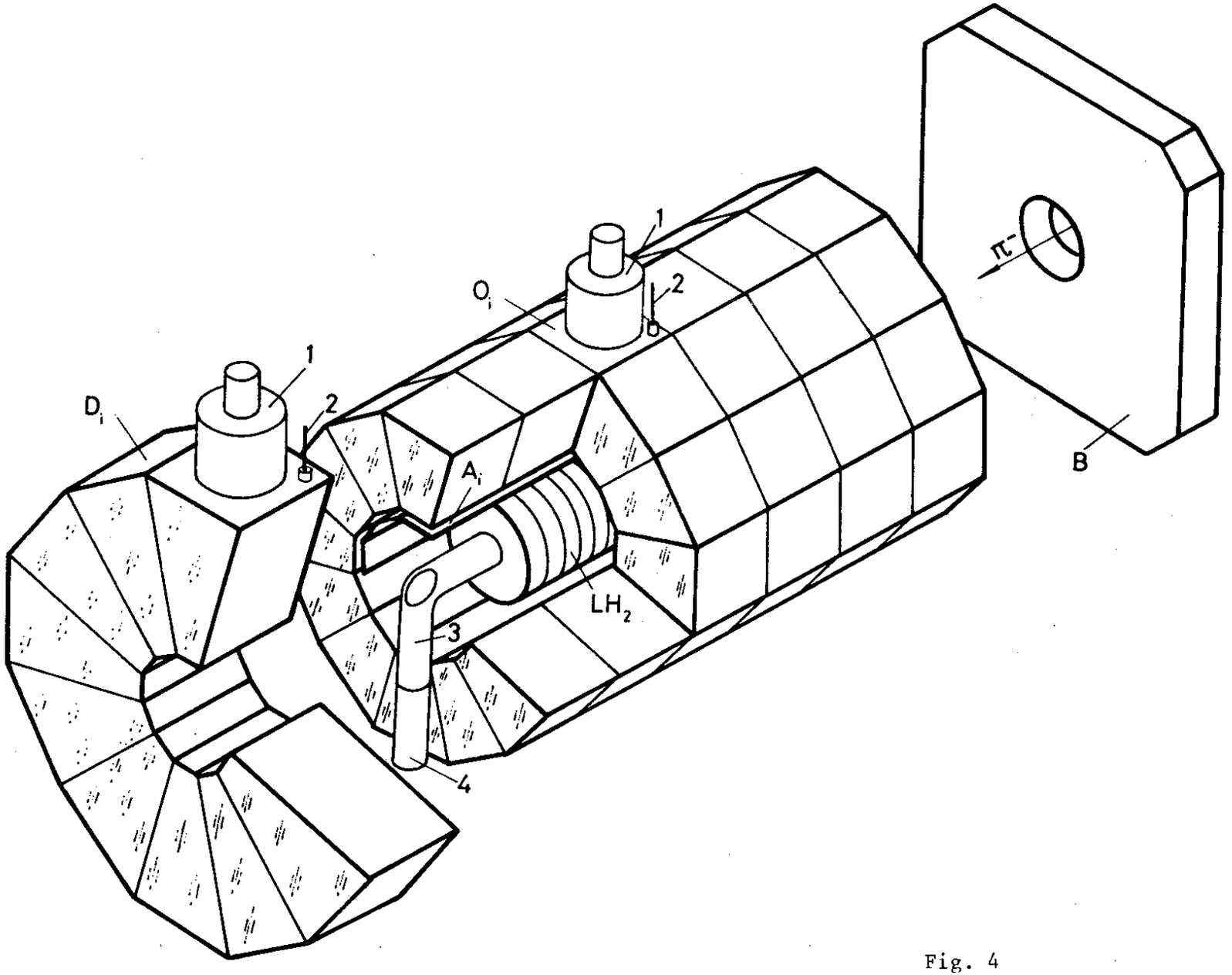


Fig. 4

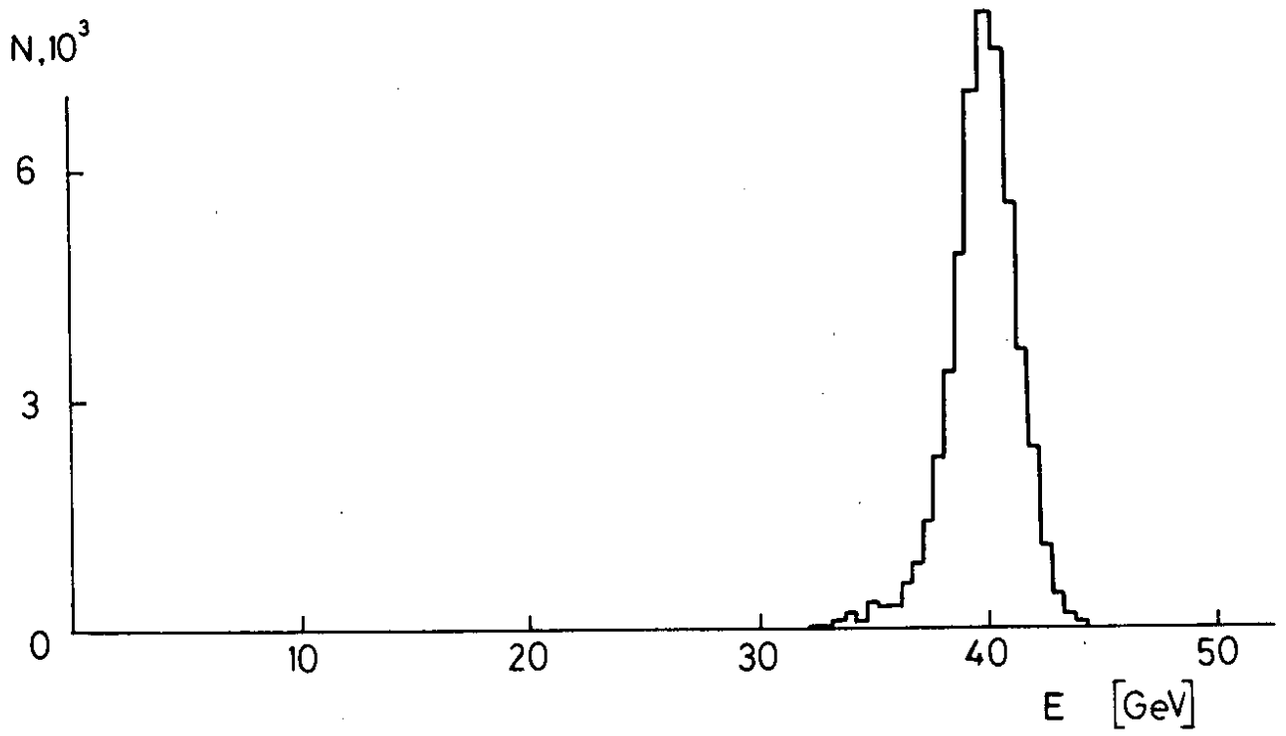


Fig. 5

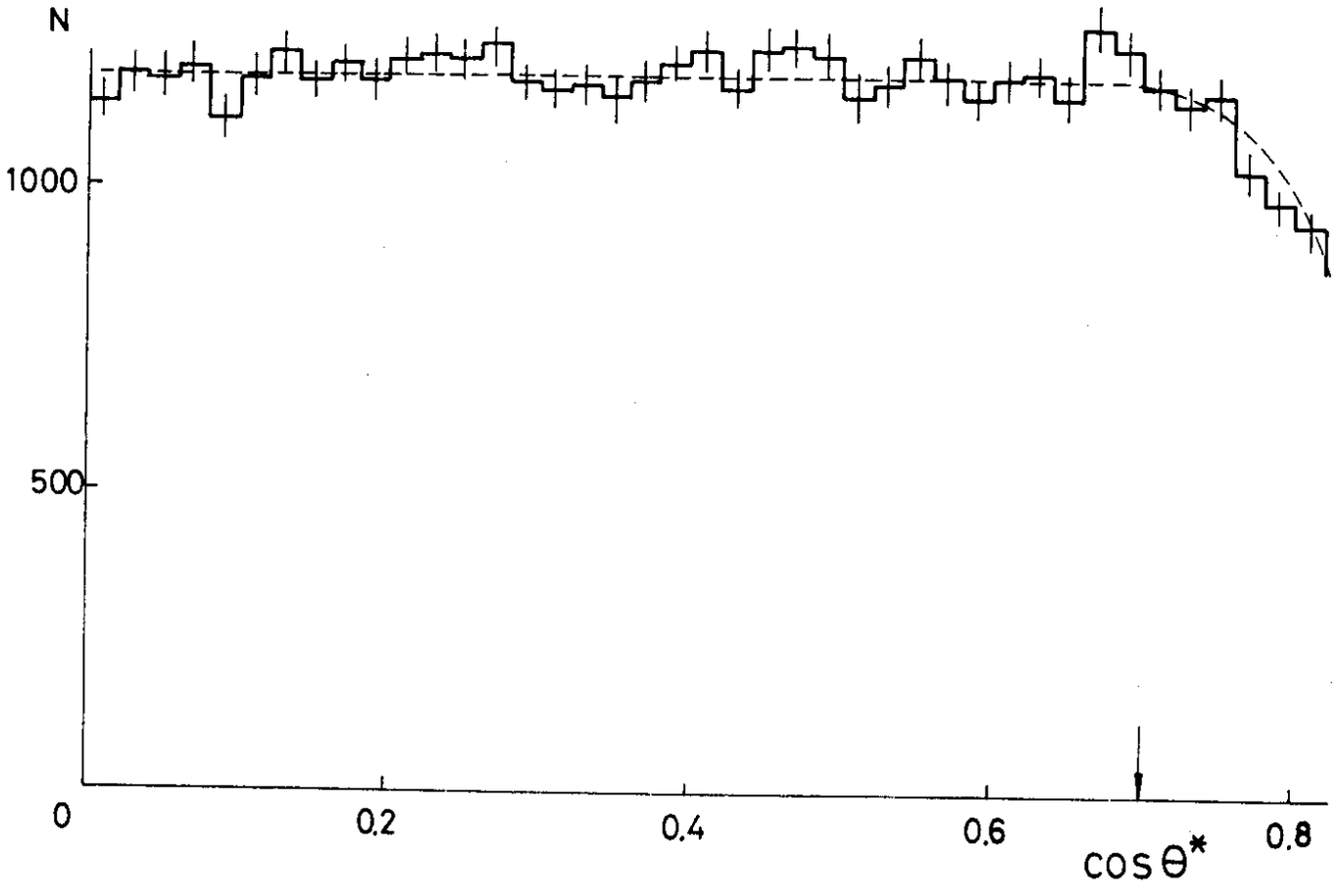


Fig. 6

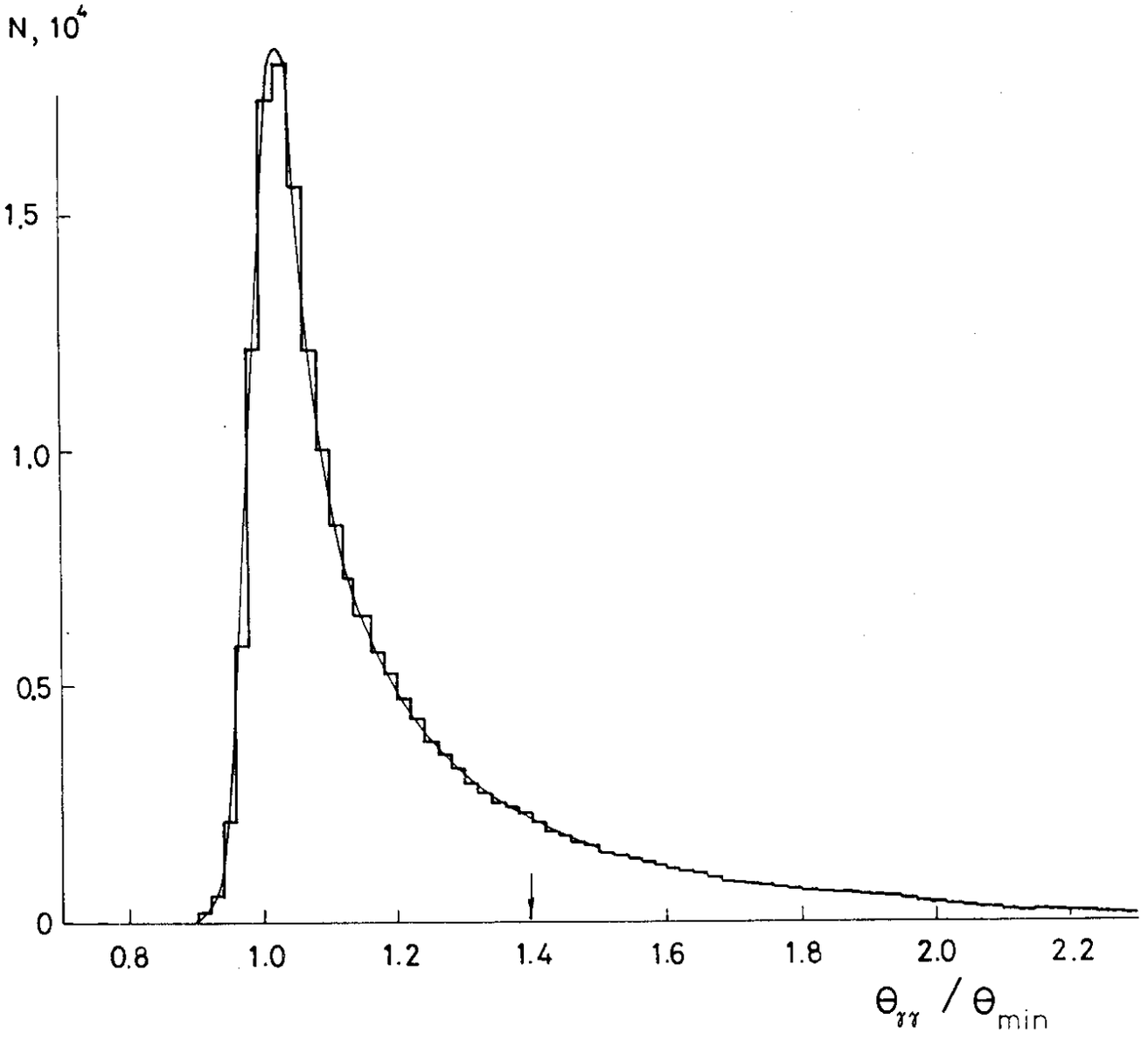


Fig. 7

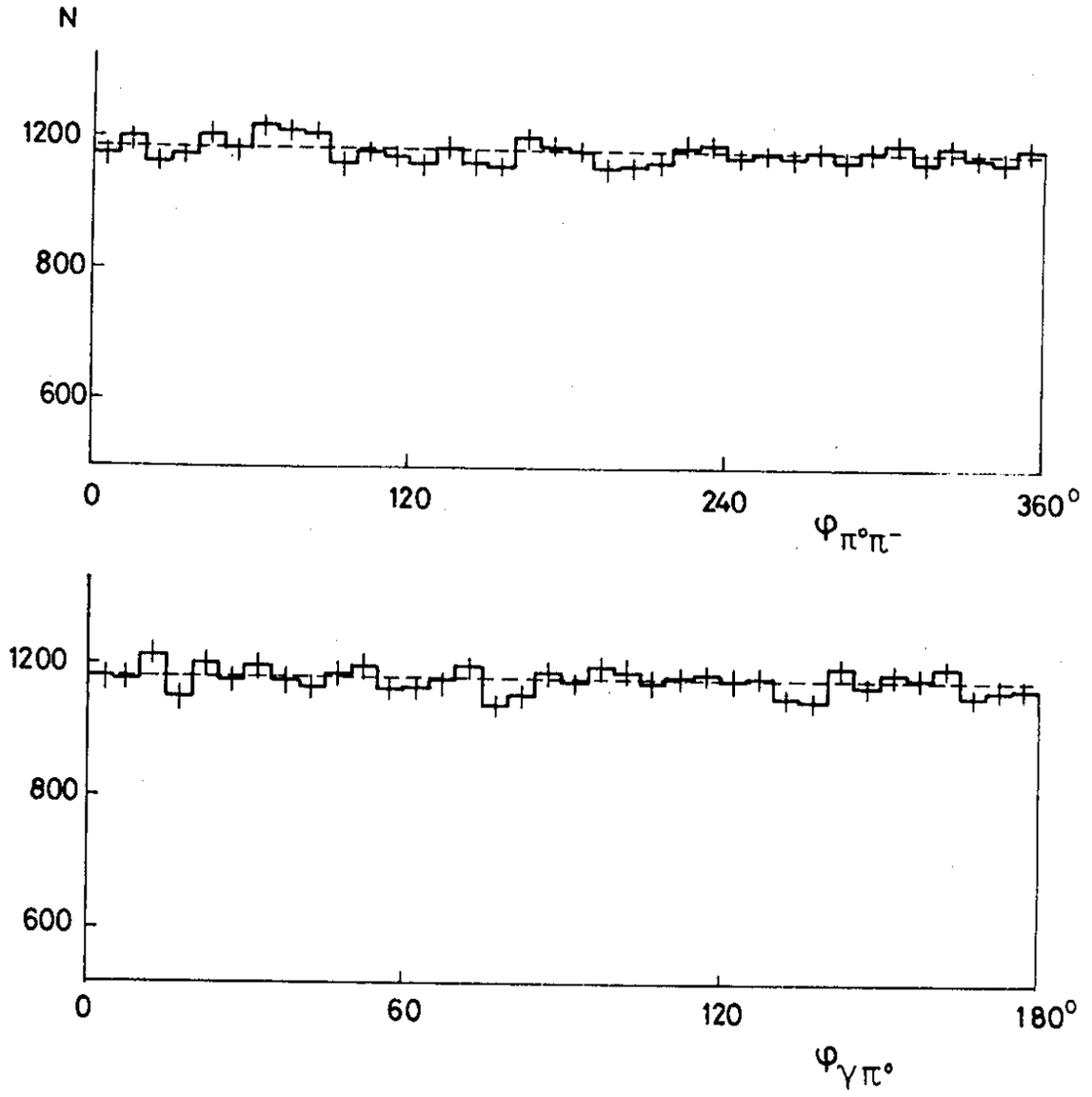
N
1200
800
600
0
120
240
360°
$\varphi_{\pi^0\pi^-}$
1200
800
600
0
60
120
180°
$\varphi_{\gamma\pi^0}$

Fig. 8

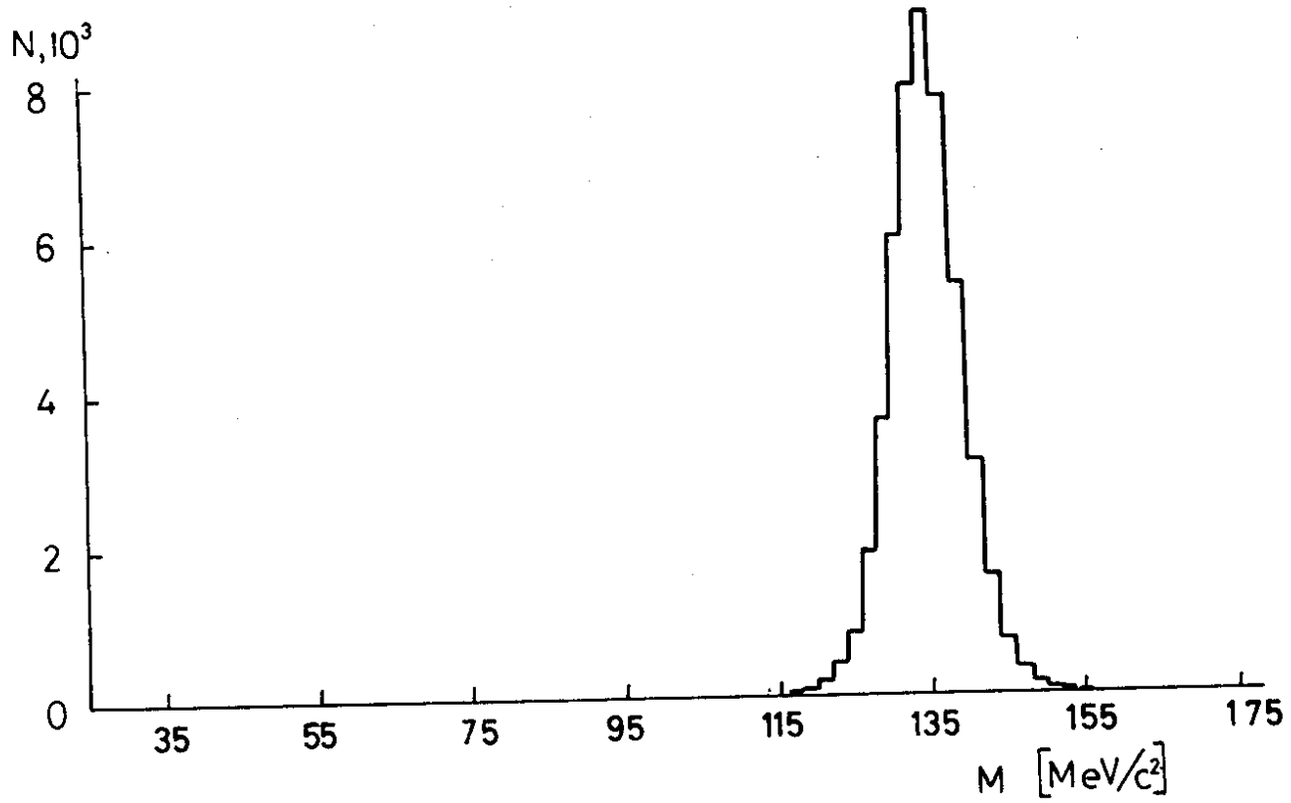


Fig. 9

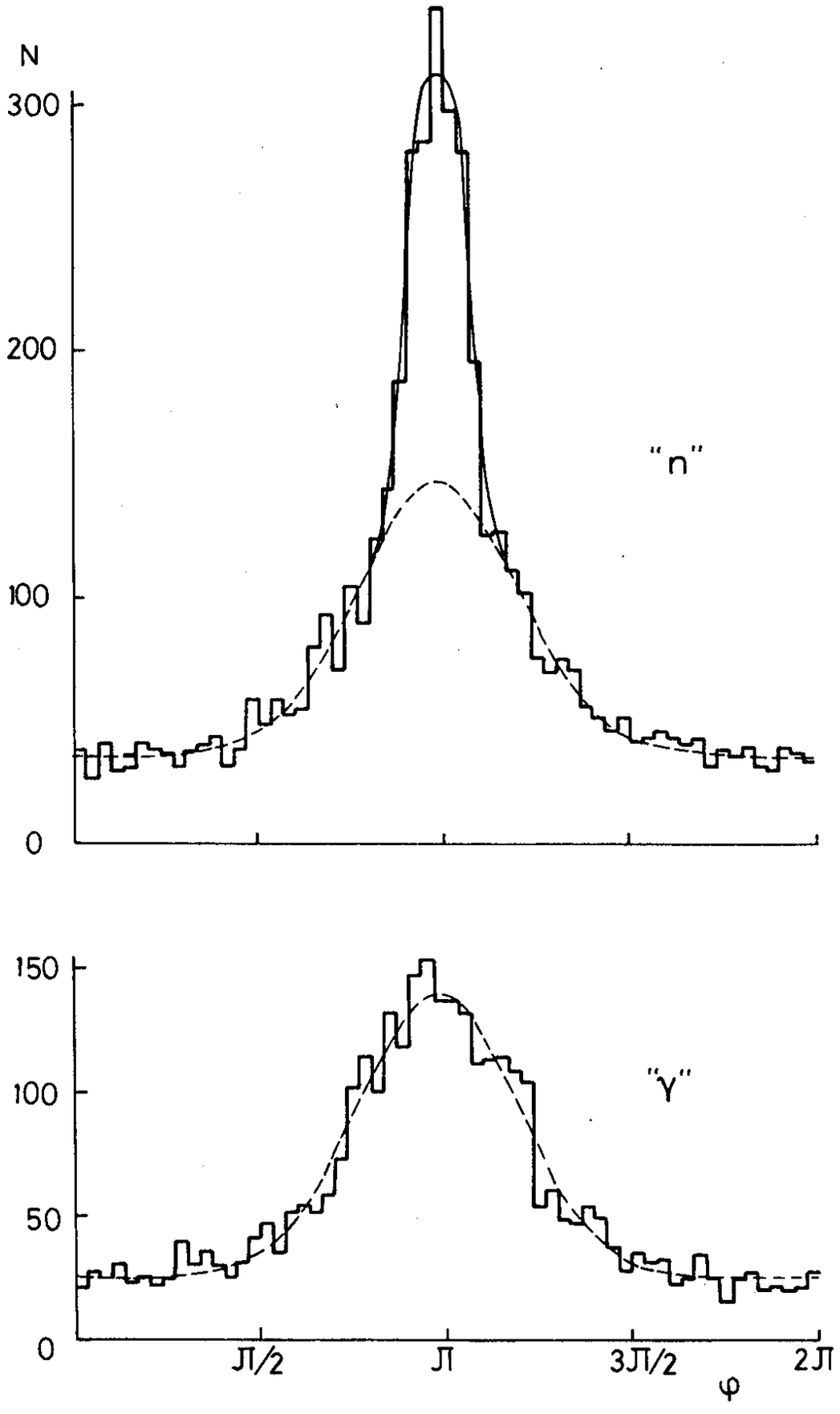


Fig. 10

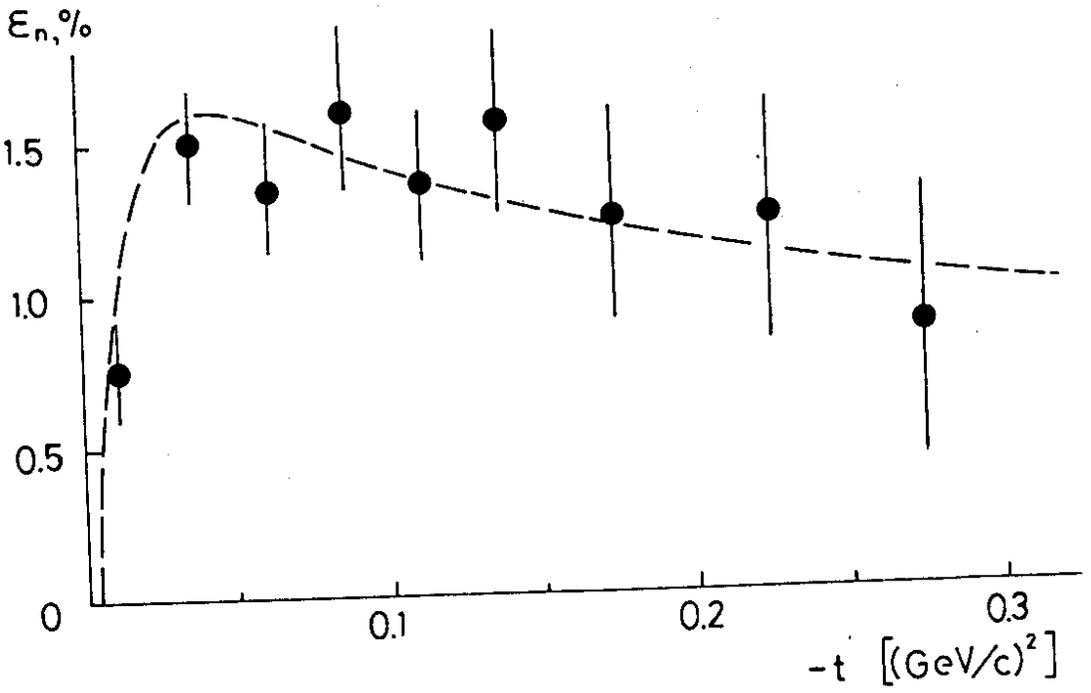


Fig. 11

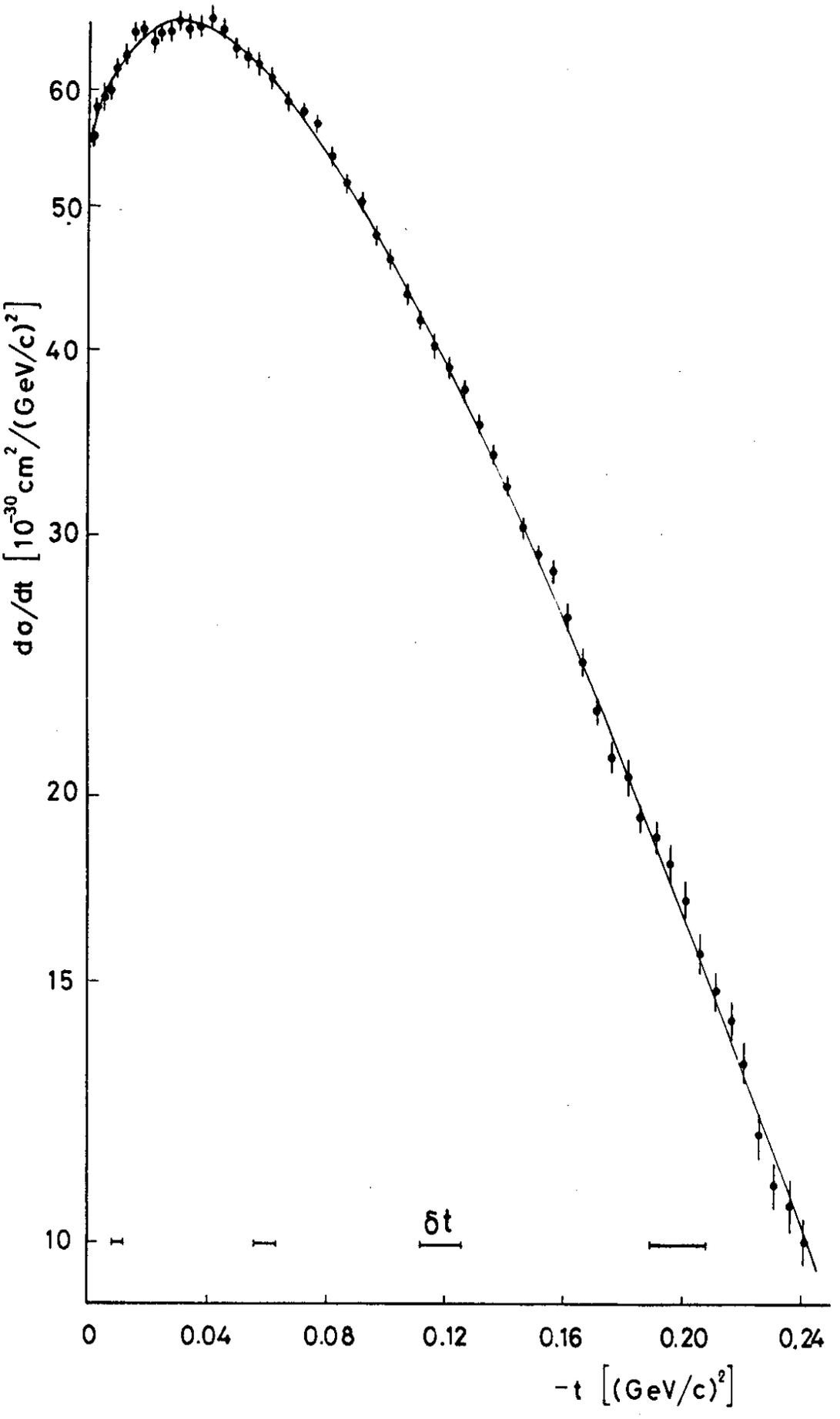
60
50
40
30
20
15
10
dσ/dt [10^-30 cm^2/(GeV/c)^2]
δt
0
0.04
0.08
0.12
0.16
0.20
0.24
-t [(GeV/c)^2]

Fig. 12